Fast tuneable InGaAsP DBR laser using quantum confined Stark effect induced refractive index change

Marianna Pantouvaki, Cyril. C. Renaud, Paul Cannard, Michael J. Robertson, Russell Gwilliam and Alwyn J. Seeds

***Abstract*— We report a monolithically integrated InGaAsP DBR ridge waveguide laser that uses the quantum confined Stark effect (QCSE) to achieve fast tuning response. The laser incorporates three sections, a forward biased gain section, a reverse biased phase section and a reverse biased DBR tuning section. The laser behaviour is modelled using transmission matrix equations and tuning over ~ 8 nm is predicted. Devices were fabricated using post-growth shallow ion implantation to reduce the loss in the phase and DBR sections by quantum well intermixing. The lasing wavelength was measured while varying the reverse bias of the phase and DBR sections in the range 0 V to < -2.5 V. Tuning was non-continuous over a ~ 7 nm wavelength range, with a side-mode suppression ratio of ~ 20 dB. Coupled cavity effects due to the fabrication method used introduced discontinuities in tuning. The frequency modulation (FM) response was measured to be uniform within ± 2 dB over the frequency range 10 MHz to 10 GHz, indicating that tuning times of 100 ps are possible.**

***Index Terms*— Tuneable semiconductor lasers, quantum confined Stark effect, quantum well intermixing (QWI), laser tuning, integrated optics, ion implantation.**

I. Introduction

Tuneable lasers attract interest for future wavelength division multiplexed (WDM) optical networks because of the potential to reduce the spares inventory, increase system flexibility and reduce system cost. Wide tuning ranges and fast tuning are desirable for a variety of applications such as optical packet switching, remote dynamic bandwidth allocation, optical frequency modulation (FM) or rapid link restoration upon network failure [1-3], thereby increasing the network flexibility and resource utilisation.

Conventional tuneable lasers utilise current injection in multiple sections to induce refractive index changes in the laser cavity and tune the lasing wavelength. Distributed Bragg reflectors (DBRs) are typically used to provide filtering of the laser cavity modes and select one mode from the spectrum, as they offer larger tuning ranges relative to distributed feedback lasers. Devices incorporating more complex multiple tuning sections (e.g. periodically sampled grating elements) such as the sampled-grating DBR laser (SG-DBR) [4], the super-structure grating DBR laser (SSG-DBR) [5], and the grating-assisted codirectional coupler with sampled reflectors (GCSR) [6, 7] have demonstrated wide tuning ranges (> 40 nm) and high unwanted mode suppression. However, the tuning speed of lasers based on current injection depends on the carrier density changes required to obtain tuning and is limited by the carrier lifetime in the passive (non-amplifying) sections. Wide tuning ranges require large current changes in the passive sections, resulting in increased switching times, particularly when switching occurs due to a change from high to low current [8, 9]. Tuning times of several nanoseconds are typical for such lasers [9-12]. Another consequence of the large current changes required for wide wavelength tuning range is heating of the device. Thermal effects cause significant wavelength drifts of microsecond timescales, which can degrade system performance [13, 14].

An alternative way to induce refractive index changes in the laser cavity is by applying a reverse bias to the tuning sections and utilising field effects such as the Franz-Keldysh (FK) and the Quantum Confined Stark Effect (QCSE). These effects are based on the absorption edge change in the presence of an electric field, which affects the complex dielectric constant of the semiconductor material at wavelengths close to the band-gap. The FK effect relates to bulk material, while QCSE occurs in structures containing quantum wells. Switching using these effects is not limited by the carrier lifetime, but by the capacitance of the device, making the technique promising for faster switching times. In addition, the lower amount of current in the laser cavity has the potential to reduce thermal effects associated with high current, and the accompanying problems

Manuscript received to be completed. This work was supported by the United Kingdom Engineering and Physical Science Research Council (EPSRC) under the Photonics component Research for Integrated Nanotechnology and Communication Environments (PRINCE) project.

Marianna Pantouvaki, Cyril C. Renaud, and Alwyn J. Seeds are with the department of Electronic and Electrical Engineering at University College London, Torrington Place, London, WC1E 7JE UK (phone: 00442076794464; fax: 00442073889325; e-mail: c.renaud@ee.ucl.ac.uk).

Michael Robertson and Paul Cannard are with the Centre for Integrated Photonics, Ipswich, IP5 3RE, United Kingdom

Russell Gwilliam is with the Advanced Technology Institute, University of Surrey, Guildford, GU2 7XH, UK.

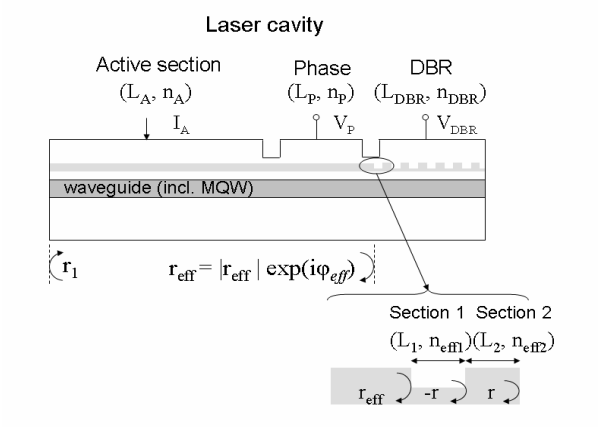

Fig. 1. Schematic of the QCSE-tuned laser.

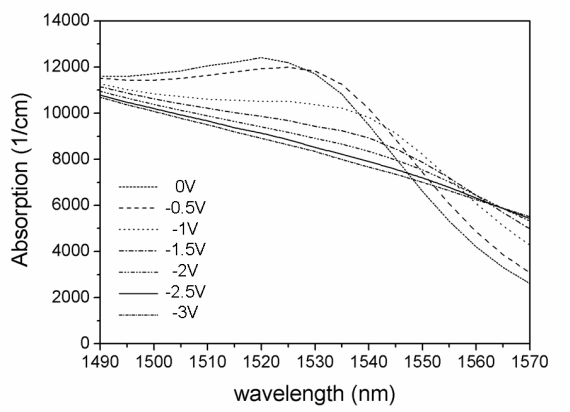

Fig. 2. Absorption spectra for the QW structure of Fig. 6 with electric field.

of wavelength drift.

Wavelength tuning based on the FK effect has been demonstrated within 500 ps across 2.5 nm wavelength range, in a butt-jointed structure realised by selective area epitaxy re-growth [15]. Although an improved design utilising a super-structure grating was proposed to increase the tuning range, the low refractive index changes induced by the FK effect (in bulk material) ultimately limit the tuning range to ~ 11 nm [16]. Using the QCSE is a more promising approach due to the sharper excitonic absorption peak in quantum well structures that results in higher refractive index changes in the material. QCSE tuning was initially demonstrated in an external cavity laser [17], and later in a tuneable twin-guide DFB laser structure with InGaAsP bulk active region and separate MQW tuning section [18], and in a butt-joined DBR laser with an MQW tuning region realised during separate growth steps [19], resulting in FM responses of < 5 GHz. In [20], we demonstrated an integrated two-section GaAs/AlGaAs laser cavity without DBR that was tuned utilising the QCSE. In this paper we present a monolithically integrated three-section InGaAsP QCSE-tuned DBR laser structure. Reverse bias is applied to both the DBR and the phase sections to control the lasing wavelength, with constant current on the gain section. The active and passive sections use the same multiple quantum well (MQW) material, while the absorption in the passive sections has been reduced via quantum well intermixing (QWI). QWI based on ion implantation is applied after complete growth of the structure. The technique has the advantage that only one epitaxial re-growth is required after the formation of the DBR, maintaining the simplicity of the fabrication process. Using this device, non-continuous tuning is demonstrated over ~ 7 nm by varying the reverse bias from 0 V to -2.5 V, with a side-mode suppression ratio (SMSR) of ~ 20 dB, and tuning times < 3 ns limited by the driving source used. FM frequency response measurements indicate that wavelength switching speeds of 100 ps are possible with this device. Significant improvements in the tuning range and SMSR can be accomplished by changing the DBR design.

The remainder of the paper is organised as follows: The QCSE tuning is modelled in Section II using experimental absorption measurements. The device fabrication and quantum well intermixing process are described in Section III. Section IV describes static and dynamic measurements on the QCSE DBR laser. Conclusions from the work are presented in Section V.

II. QCSE-Tuned Laser Theory

The schematic of the QCSE-tuned DBR laser is shown in Fig. 1. The device comprises an active section that provides the gain, and two passive sections, namely the phase and the DBR. The three sections are electrically isolated and individually biased. A constant current is applied to the active section, while the phase and DBR sections are reverse biased. The waveguide region includes an MQW structure that is common for all sections but is quantum well intermixed in the passive sections to reduce the loss. The grating section is a periodic DBR structure, formed on an InGaAsP layer above the waveguide region. Details on the device structure and fabrication are given in Section III.

A. QCSE refractive index changes

When a voltage is applied perpendicular to a p-i-n structure with an MQW, the energy band-gap is tilted and the wavefunctions of the electrons and holes in the wells are pulled apart, causing the exciton absorption peaks to red-shift and the exciton oscillator strength to reduce. This is the Quantum Confined Stark Effect [21]. The refractive index changes that accompany the absorption changes can be used to modify the light path in a multi-section tuneable laser, tuning the wavelength of the output light. Fig. 2 shows the variation of the absorption spectrum of an intermixed, strain-balanced InGaAsP MQW laser structure such as that described in Section III. The absorption spectrum was calculated from photocurrent measurements under the effect of an electric field, with light incident normal to the wafer, using the equation

$$\alpha_m = -\frac{1}{d}\ln\left(1-\frac{hc\ I_{ph}}{e\ \eta\ P_{ip}\ (1-R)\ \lambda}\right) \quad (1),$$

where $\alpha_m(\lambda)$ is the material absorption, d is the thickness of the quantum wells, h is Planck's constant, c is the speed of

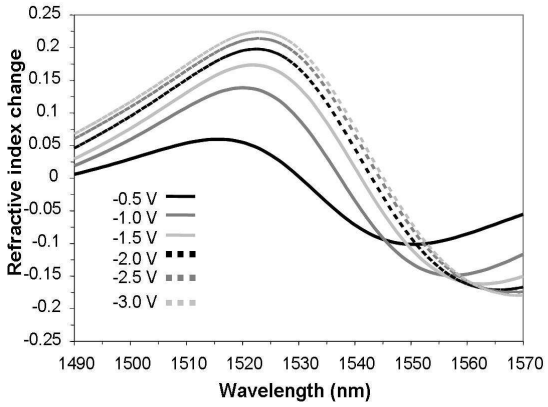

Fig. 3. Refractive index change due to electric field derived from data of Fig. 2. The changes quoted are with reference to the zero-field case.

light in vacuum, I_{ph} is the photocurrent, e is the electron charge, η is the quantum efficiency, where η = 0.9 was used, P_{ip} is the incident optical power, R is the reflectivity of the air-semiconductor interface and λ is the wavelength.

The absorption changes observed with increasing magnitude of reverse bias result in refractive index changes that can be calculated by the Kramers-Kronig equation [22]:

$$\Delta n_m(\lambda, E) = \frac{\lambda^2}{2\pi^2} P \int_0^\infty \frac{\Delta \alpha_m(\lambda', E)}{\lambda^2 - \lambda'^2} d\lambda' \quad (2),$$

where E is the electric field, P is the Cauchy principal value of the integral, and $\Delta\alpha_m$ and Δn_m are the material absorption and refractive index changes respectively relative to zero electric field, both depending on the electric field and the wavelength. Fig. 3 presents the refractive index change spectrum (Δn_m) calculated from (2) using the absorption spectra of Fig. 2. Though, there is a wide spectral range where QCSE-induced refractive index changes could be used, their amplitude varies with wavelength. Significant refractive index changes are observed at longer wavelengths than the exciton absorption peak. For this spectral range the absorption and absorption changes due to QCSE are lower. A device with intermixed passive sections can take advantage of this as its exciton absorption peak will be blue shifted. In that case, lasing occurs at wavelengths longer than that of the exciton absorption peak of the passive sections. Furthermore, as absorption changes due to QCSE will remain small, tuning of the lasing wavelength is possible without suffering large variations of the laser output power.

B. Tuning mechanism

The wavelength tuning due to refractive index changes in the DBR section can be calculated using the transmission matrix theory [23]. The transmission matrix for a single period of the DBR, comprising the two sections of lengths L_1 and L_2 as shown in Fig. 1, is

$$T_P = \begin{bmatrix} T_{P11} & T_{P12} \\ T_{P21} & T_{P22} \end{bmatrix} \quad (4),$$

where

$$T_{P11} = \left(e^{i\varphi_1} - r^2 e^{-i\varphi_2}\right)/t^2 \quad (5),$$

$$T_{P12} = r\left(e^{-i\varphi_1} - e^{i\varphi_2}\right)/t^2 \quad (6),$$

$$T_{P21} = r\left(e^{i\varphi_1} - e^{-i\varphi_2}\right)/t^2 \quad (7),$$

$$T_{P22} = \left(e^{-i\varphi_1} - r^2 e^{i\varphi_2}\right)/t^2 \quad (8)$$

and

$$\varphi_1 = \beta_1 L_1 + \beta_2 L_2 \quad (9),$$

$$\varphi_2 = \beta_1 L_1 - \beta_2 L_2 \quad (10),$$

β_1 and β_2 are the complex propagation constants in the sections 1 and 2 and are given by

$$\beta_{1,2}(\lambda, V) = \frac{2\pi}{\lambda} n_{1,2}(\lambda, V) - i\frac{\alpha(\lambda, V)}{2} \quad (11),$$

where $\alpha(\lambda) = \Gamma_{QW}.\alpha_m$, Γ_{QW} is the confinement factor of the QWs, and $n_1(\lambda,V)$ and $n_2(\lambda,V)$ are the effective indices of the dielectric sections of length L_1 and L_2 that constitute the grating. The wavelength and voltage dependence of these effective indices can be written as

$$n_{1,2}(\lambda, V) = n_{eff\,1,2}(\lambda) + \Delta n_{1,2}(\lambda, V) \quad (12),$$

where n_{eff1} and n_{eff2} are the effective indices at 0 V bias of the two segments that comprise the DBR. The wavelength dependence of the refractive indices is calculated as described in [24]. The change of the effective refractive indices with voltage is approximated as $\Delta n_1(V) = \Delta n_2(V) = \Gamma_{QW}\Delta n_m(V)$, where Δn_m is calculated from equation (2) and absorption measurements. In equations (5)-(8), the reflectivity and transmission coefficients of the interface between the two sections are

$$r = \frac{n_2 - n_1}{n_2 + n_1} \text{ and } t = \sqrt{1 - r^2} \quad (13)$$

The transmission matrix of a DBR of N periods, is then given by

$$T_G = \begin{bmatrix} T_{G\,11} & T_{G\,12} \\ T_{G\,21} & T_{G\,22} \end{bmatrix} = T_P{}^N \quad (14)$$

and the reflectivity of the DBR can be calculated from

$$R_{DBR} = \frac{T_{G\,21}}{T_{G\,11}} \quad (15).$$

Fig. 4 shows the wavelength tuning ($\Delta\lambda_G$) of the central wavelength of the DBR (λ_G) with applied voltage on the DBR section, calculated as described above. The wavelength tuning is given by $\Delta\lambda_G = \lambda_G(V) - \lambda_{G0}$, where λ_{G0} and $\lambda_G(V)$ are the wavelength of the DBR at 0 V and at voltage V, respectively. In Fig. 4, $\Delta\lambda_G$ is calculated for different positions of the DBR central wavelength relatively to the MQW exciton wavelength. This is expressed by $\delta\lambda_{G0} = \lambda_{G0} - \lambda_{exc}$, that is the difference between the DBR central wavelength at 0 V (λ_{G0}) and the wavelength of the exciton absorption peak (λ_{exc}). $\delta\lambda_{G0} = 0$ nm

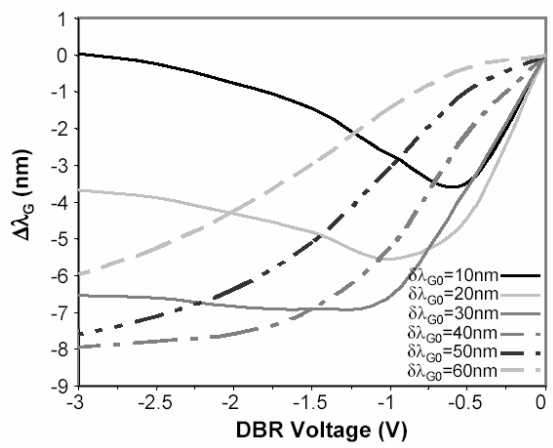

Fig. 4. Tuning of the DBR central wavelength versus DBR voltage for various detunings from the exciton absorption peak.

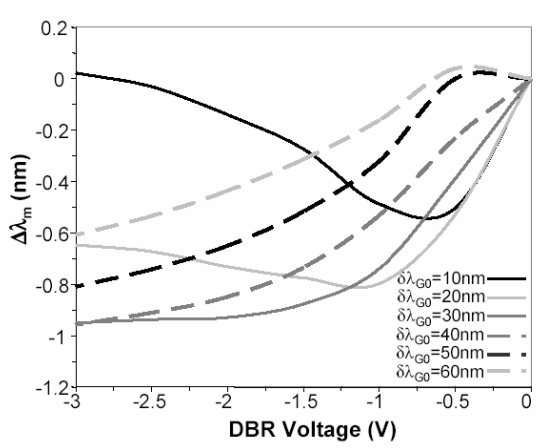

Fig. 5. Tuning versus phase voltage for various detunings from the exciton absorption peak.

occurs when the DBR wavelength at 0 V coincides with the wavelength of the excitonic absorption peak. At $\delta\lambda_{G0}$ = 10 nm the DBR central wavelength is positioned 10 nm longer than the exciton peak, etc. The QCSE wavelength dependence suggests that the tuning of the DBR mirror ($\Delta\lambda_G$) depends on $\delta\lambda_{G0}$, because of the variations of the refractive index changes with wavelength. However, Fig. 4 shows that > 6 nm (and up to ~ 8 nm) tuning is possible across ~ 30 nm with the structure used in this work, indicating that tuning ranges > 30 nm could be achieved if the device design was modified to include multiple tuning sections (e.g. SG-DBR).

Having calculated the reflectivity and the phase of the DBR section, the tuning of the lasing wavelength due to the phase section can be found from

$$\frac{\Delta\lambda_m}{\lambda_m} = \frac{\left(\Delta n_A L_A + \Delta n_P L_P + \Delta n_{DBR} L_{eff,DBR}\right)}{\left(n_A L_A + n_P L_P + n_{DBR} L_{eff,DBR}\right)} \qquad (16),$$

where λ_m is the lasing wavelength of the mode, n_A, n_P and n_{DBR} are the effective refractive indices of the active, the phase and the DBR sections respectively; L_A, and L_P are the length of the active and the phase sections, and $L_{eff,DBR}$ is the effective length of the DBR, which is given by

$$L_{eff,DBR} = \frac{1}{2}\frac{d\varphi_{eff}}{d\lambda}\frac{\lambda^2}{2\pi\, n_G} \qquad (17),$$

where φ_{eff} is the phase of the DBR reflectivity, as shown in Fig. 1. For constant current applied to the active section and constant voltage on the DBR, this can be written as

$$\frac{\Delta\lambda_m}{\lambda_m} = \frac{\Delta n_P L_P}{\left(n_A L_A + n_P L_P + n_{DBR} L_{eff,DBR}\right)} \qquad (18).$$

Fig. 5 shows the mode tuning due to the phase section calculated from (18). It was found that changing the phase from 0 V to -3 V fine tunes the laser wavelength by < 1 nm.

III. Device Description

A. Epitaxial structure

The structure, the schematic cross-section and a top picture of the fabricated QCSE DBR laser are shown in Fig. 6. The wafer was grown by metal-organic vapour phase epitaxy (MOVPE) on a semi-insulating InP substrate. The waveguide region incorporates eight 7 nm-wide compressively strained InGaAsP (λ_g = 1.65 μm) quantum wells and seven 14 nm-wide tensile strained InGaAsP (λ_g = 1.3 μm) barriers, sandwiched between two InGaAsP (λ_g = 1.3 μm) waveguide layers. Above the waveguide region, a 170 nm-InP spacer layer and a 30 nm InGaAsP (λ_g = 1.3 μm) grating layer, both p-doped, were grown. The growth was interrupted at this stage and a first-order grating was formed on the InGaAsP layer in the area required for the DBR section. The structure was completed by the overgrowth of a 1.4 μm p-InP layer, a 0.2 μm p-InGaAs contact layer, a 0.5 μm InP implantation buffer layer and a final 0.1 μm InGaAs implantation buffer layer. Following growth, the tuning sections were quantum well intermixed using ion implantation, as described in the next section.

B. Post-growth Quantum Well Intermixing

In the QCSE DBR laser the gain and the passive sections utilise the same MQW area. As a consequence, the absorption peak of the passive sections is close to the lasing wavelength, introducing significant loss. To reduce the absorption experienced by the light generated in the active section and transmitted through the tuning sections, we used post-growth quantum well intermixing (QWI) to blue-shift the band-gap of the passive sections. In QWI, partial mixing of the elements of

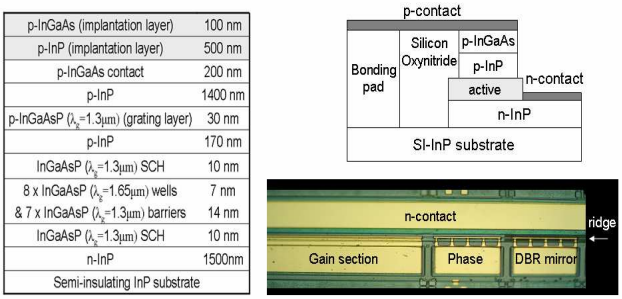

Fig. 6. Wafer structure, schematic cross-section and top picture of the QCSE DBR laser. The top InP and InGaAs implantation layers (in grey) are removed after intermixing and before further processing.

the wells with those of the barriers can increase the energy band-gap of the wells and blue-shift the photoluminescence peak. The shift depends on the extent of intermixing, which can be varied by changing different parameters of the method used. The advantage of post-growth QWI compared to selective area epitaxy re-growth is that it is less complex to use, particularly when the passive sections incorporate QWs, while it can also be used to create multiple band-gap detunings on the same wafer in a single QWI step [25].

There are a few techniques that have been used to achieve QWI, such as impurity-free vacancy disordering (IFVD) [25-28], impurity-induced disordering (IID) [29], laser-induced disordering [30], and ion implantation [31-34]. In this paper we apply shallow ion implantation of P^+ ions followed by thermal annealing [31, 32]. In contrast to high energy implantation, shallow implantation introduces defects above the cladding, which are then diffused into the quantum wells during annealing. If a sacrificial implantation buffer layer is used, the implantation energy can be chosen so that the ions stop in this layer, which can be removed after annealing, leaving the material free of implanted ions. Compared to deep implantation, shallow implantation can therefore maintain better material crystalline quality. In the past, this method was used to intermix partially grown structures, while the remaining p-doped top layers were over-grown after intermixing and removing the implantation buffer layer [32, 34]. This was done to prevent diffusion of the p-dopants into the laser active region during thermal annealing, and hence performance degradation. In this paper we use shallow ion implantation followed by rapid thermal annealing at 650^0C to blue-shift the passive sections after completion of growth of the full structure. The method uses implantation buffer layers of different material composition to vary the degree of intermixing and can be applied to achieve multiple band-gap detunings on the sample during the same QWI step.

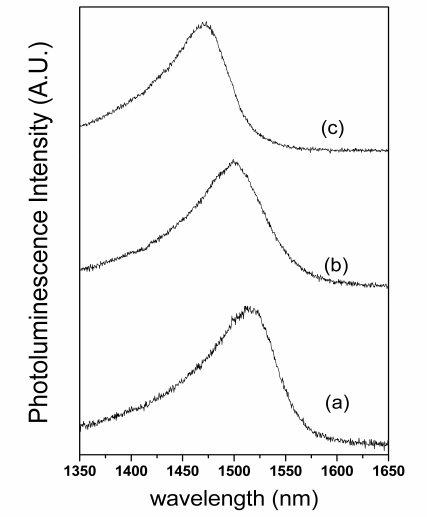

Fig. 7. Room temperature photoluminescence spectra after implantation and annealing at 650^0C for 5 min, from (a) the unimplanted laser section, (b) the passive sections with an InP cap and c) the passive sections with an InGaAs cap.

When implantation is used for QWI, the band-gap detuning can be varied by changing the implantation energy, the dose, the annealing time or temperature. In particular, increasing the annealing temperature enhances the intermixing, but also increases the risk for Zn diffusion. Varying the material of the top buffer layer provides yet another parameter for band-gap detuning control, because the types of defects generated in the material during implantation depend on the material composition itself. Increased bandgap blue-shifts have been reported using an InGaAs cap layer, compared to an InP cap, below the SiO_2 layer in IFVD [27, 28]. In order to investigate this in the case of shallow implantation and to select the final conditions for the QCSE-tuned lasers, we performed calibration runs using only the InP or both the InGaAs and InP implantation buffer layers of the structure of Fig. 6. To prevent Zn diffusion and blue-shifting in the active section, annealing was performed at 650^0C temperature.

Samples from the wafer structure described in the previous section were cleaved and the InGaAs cap layer was removed from half of them, using selective wet etching. The gain section of both types of samples was then covered with 600 nm SiO_2 deposited using plasma-enhanced chemical vapour deposition (PECVD) to prevent intermixing of the area. The samples were subsequently implanted with P^+ ions at 100 keV energy and 200^0C temperature, at dose $8x10^{14}$ cm^{-2}. After implantation, annealing was performed at 650^0C for various times. During rapid thermal annealing, a clean polished InP substrate was used as the proximity cap. A comparison of the effect of the top layer composition was also performed. An example of the photoluminescence shift of two passive sections with InP only and InP plus a small InGaAs caps, both annealed for 300 s at 650^0C, is shown in Fig. 7. The photoluminescence of the active section after the QWI process is also shown for comparison. It was found that, for the same QWI conditions, the samples with the InGaAs cap resulted in higher band-gap detuning of the implanted material, while in both cases, the photoluminescence shift of the unimplanted gain section was negligible. Fig. 8(a) shows in more detail the band-gap detuning for samples with an InP or InGaAs cap as a function of annealing time. There have been a number of theories on how intermixing takes place in InGaAsP, and band gap detuning has been ascribed to the interdiffusion of both group III and group V defects [27, 28, 33]. Fig. 8(b) shows the damage induced by implantation with only the InP and with both the InGaAs and InP implantation layers on top of the basic laser structure. The simulation was performed using TRIM [35], which does not account for high-temperature implantation effects, but nevertheless gives an insight of the damage produced during implantation. Although with the InGaAs cap the peak of the distribution of defects is further away from the active region, the number of calculated defects generated in this case is almost double, as confirmed by the larger detuning measured (Fig. 8(a)).

After the calibration runs for the QWI process, samples with the InGaAs cap that would be processed into QCSE-tuned lasers were covered with PECVD SiO_2, implanted using the

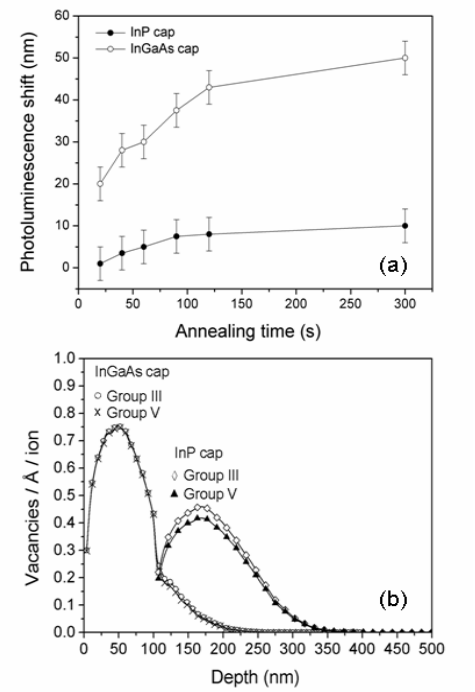

Fig. 8. a) Wavelength detuning of the photoluminescence peak of the implanted sections as a function of annealing time, for annealing at 650^0C. b) Simulation of the group III and V vacancies created during implantation through a top InGaAs and a top InP cap layer.

same conditions as above and annealed at 650^0C for 90 s. In this way, the photoluminescence peak of the passive sections was blue-shifted by ~ 37 nm compared to the gain section, in the final devices. Following fabrication, the samples were cleaved to form devices with 1 mm long gain section, 170 μm long phase section and 160 μm long DBR section. The output light from each facet was measured as a function of current in the gain section, for a non-intermixed and an intermixed device and is shown in Fig. 9. For these measurements, the passive sections were kept at 0 V bias. Significant reduction of the loss experienced by light output from the DBR facet is observed after QWI. A somewhat higher annealing time could result in even lower loss. The lasing threshold was only slightly increased after QWI, while mode hopping was observed with increasing current in both cases, due to changes in the laser cavity phase with increasing current.

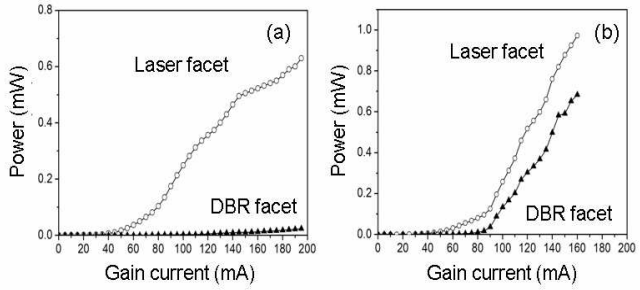

Fig. 9. Laser output power versus gain current plot for a) a QCSE DBR laser that has not been intermixed, and b) a QW intermixed QCSE DBR laser.

C. *Device fabrication*

After growth and intermixing, the wafer was processed into ridge waveguide lasers, with three sections, the gain, the phase, and the DBR mirror. Both the p-and n-contacts were formed on top of the wafer, while bridges on silicon oxynitride were used to connect the p-contact to the bonding pads to reduce the device capacitance. The measured capacitance of the device was ~ 200 fF/ 100 μm. A more detailed description of the fabrication procedure can be found in [36].

To use the QCSE as the tuning mechanism, the phase and the DBR sections need to be reverse biased, while the gain section is forward biased. In a monolithically integrated device, where the three sections have a common intrinsic region, good electrical isolation between the sections is necessary. In this work, electrical isolation between the sections was accomplished by removing the top p-InGaAs and p-InP contact layers from a 30 μm wide gap between different sections. This resulted in ~ 15 kΩ resistance between neighbouring p-contacts with the gain section unbiased. Higher contact resistance is possible by using ion implantation [15]. Neither of the facets was anti-reflection coated for the results presented in this paper.

IV. Laser Results

A. *Static measurements*

For the tuning measurements of the QCSE DBR laser, the bias current of the gain section was kept at 150 mA, while the reverse bias was varied from 0 V to - 2.5 V on the DBR, and from 0 V to -1 V on the phase section. Fig. 10 illustrates an example of the spectra measured at the output of the QCSE DBR laser. The variation of the peak output power for all the lasing wavelengths measured was < 6 dB, while the SMSR of the laser was ~ 20 dB, resulting in nontrivial mode competition. A DBR mirror with stronger filtering characteristic would be desirable. The spectra exhibit modulation of the side modes with period that agrees well with the 170 μm length of the phase section (dotted line in Fig. 10). This modulation is attributed to a secondary cavity that is formed between the two isolation gaps, one separating the phase section from the DBR mirror and the second between the phase and the gain sections, resulting in secondary minima in the spectrum, that do not allow for continuous tuning

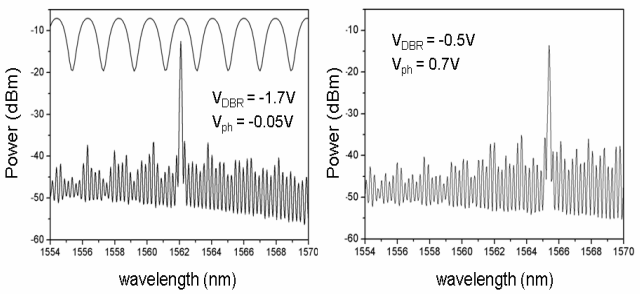

Fig. 10. Examples of the measured output spectra. The dashed line on the first figure represents the spectrum of a 170 μm long cavity.

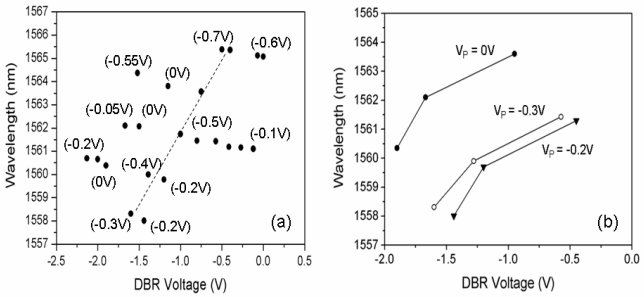

Fig. 11. a) QCSE DBR laser wavelength versus DBR voltage. The voltage applied on the phase section is shown in brackets. The dotted line shows the general trend with reducing DBR voltage for phase voltage adjusted to maintain high SMSR. b) Detail of (a), showing the tuning for fixed phase voltage (V_P), for values V_P = 0 V (●), V_P = -0.2 V (▼), and V_P = -0.3 V (○).

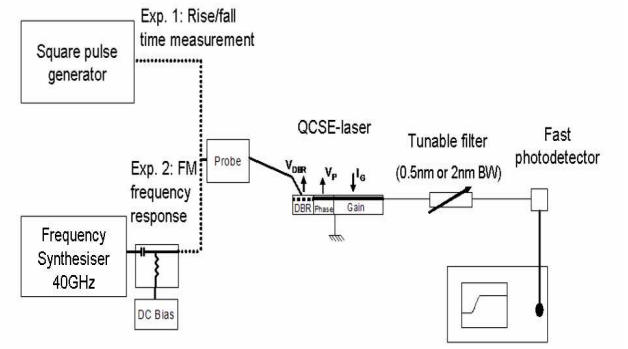

Fig. 12. Experimental configuration for dynamic measurements. The QCSE DBR laser was driven using the square pulse generator for the switching measurements and the sinusoidal frequency generator for the FM response measurement.

between the laser modes. This is due to the deep etch of the p-doped layers performed in order to electrically isolate the sections, which modified sufficiently the effective refractive index along a distance of 30 μm, to result in the formation of a secondary cavity.

In Fig. 11(a), the lasing wavelength is plotted versus DBR voltage, while the phase voltage is shown in brackets. The phase voltage was varied to optimise the SMSR. The dotted line in Fig. 11(a) shows an exemplary tuning region of high SMSR while both the grating and phase current were changed. One can note the discontinuities in the tuning map which are mainly due to lateral mode jump and the coupled cavity effects referred to above. In general, the lasing wavelength is moving towards shorter wavelengths across ~ 7 nm range, as the DBR voltage reduces. The tuning range is comparable to the calculated value of ~8 nm.

The tuning to shorter wavelength, as expected from the calculation shown in fig.4, with reducing DBR voltage is also shown in Fig. 11(b), where examples of wavelength tuning for fixed phase bias are plotted. Note that for this measurement several mode jumps where observed across the tuning range and the point given are only the one with a good SMSR. As expected from the modelling the amount of QCSE tuning does not evolve linearly with the applied voltage (Fig. 11(b)). Again it agrees well with Fig. 4, for the case that the DBR central wavelength is positioned at ~ 40 nm longer wavelength than the exciton peak ($\delta\lambda_{G0}$= 40 nm), which is the closest approximation to the final device. From Fig. 5, it was expected that the fine tuning induced by the phase section will result in shorter output wavelength when the voltage is reduced. However, from a given voltage, we observed the opposite effect (Fig. 11(b)), that the fine phase tuning was inducing a total shift towards longer wavelength. It was found that this is not due to leakage current. Alternatively, we believe that the main reason for this to occur is that reducing the phase voltage red-shifts the absorption peak towards the wavelength of interest, resulting in an increase of absorption in the phase section. This in turn reduces the light input to the DBR, which causes a decrease of the photocurrent in the DBR section. Lower photocurrent corresponds to reduced absorption and refractive index changes in the DBR section. This trend competes with the increase in absorption in the DBR due to the decrease of the DBR voltage, resulting in coarse tuning towards shorter and fine tuning towards longer wavelength.

B. Dynamic measurements

Dynamic characterisation of the QCSE DBR laser was carried out using the configuration of Fig. 12. Two kinds of experiments were performed, the first using a step voltage pulse to measure the switching speed between two lasing wavelengths, while the second was a small signal sinusoidal frequency response measurement. During both experiments, the phase section was kept at fixed reverse bias to simplify the measurement, while the DBR section tuning voltage was applied through a coplanar probe with a 65 GHz bandwidth.

In the first experiment, the DBR section was driven using a step voltage pulse, between values of the reverse bias that corresponded to two different lasing wavelengths. Since the phase voltage was not varied simultaneously with the DBR reverse bias, only a limited range of switching wavelengths, having good SMSR, were measured. The resulting optical pulse output from the QCSE DBR laser passed through an optical filter of 0.5 nm bandwidth and the rise and fall times were measured on a sampling oscilloscope with a 60 GHz photodiode. As rise or fall time, we refer to the time required

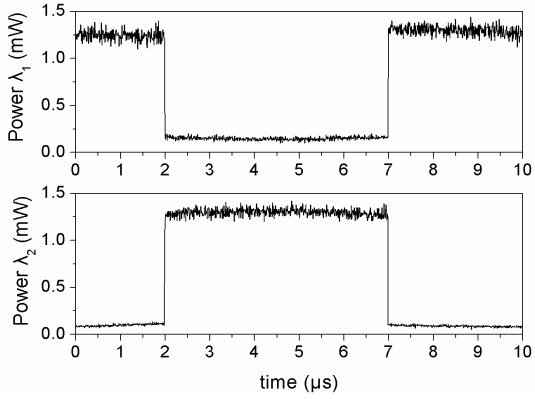

Fig. 13. Oscilloscope traces showing laser output power when switching from wavelength λ_1 and wavelength λ_2.

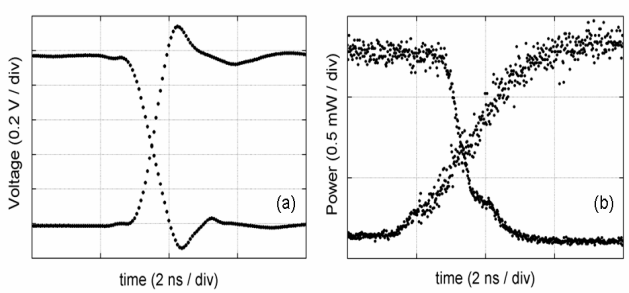

Fig. 14. a) Input square voltage pulse used for switching measurements and b) detail of laser output power at wavelength λ_2.

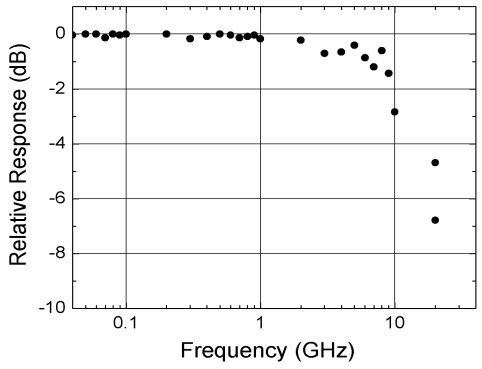

Fig. 15. FM frequency response of the QCSE tuned DBR laser.

for transition between 10 % and 90 % power at the desired wavelength. Fig. 13 shows the waveforms observed for a switching pulse of 5µs duration. For this measurement, the voltage on the phase section was kept at ~ -0.2 V and the voltage on the DBR was varied between 0.5 V and -1.2 V, resulting in wavelengths λ_1 = 1561.2 nm and λ_2 = 1559.8 nm respectively. When the optical power at wavelength λ_1 was off, lasing at the second wavelength λ_2 was being switched on. The response is seen to be free of thermal overhang. Details of the leading and falling edges of the driving voltage pulse with corresponding optical power changes are shown in Fig. 14. Although the rise and fall times of the voltage pulse source were approximately 800 ps, there was an overshoot of ~ 0.2 V of the voltage pulse before it was stabilised at the new state within ~ 3.5 ns, as shown in Fig. 14(a). This overshoot was sufficient to cause the lasing wavelength to switch outside the bandwidth of the filter used in this measurement so that the correct voltage was only achieved after ~ 3 ns. For the fall time, the voltage merely needs to change sufficiently to tune the laser out of the filter bandwidth, resulting in a much more rapid fall time for the detected optical power. It can be seen that the laser changes wavelength within 1 ns of the correct voltage being reached.

The second experiment performed for dynamic characterisation of the device was a frequency modulation frequency response measurement. In this case, the device was driven by a sinusoidal frequency generator with a peak-to-peak voltage 1 V at frequencies up to 40 GHz. The peak-to-peak value and the DC bias on the DBR section were chosen to keep the laser operation within a continuous tuning region while retaining the largest possible range of wavelength scanned. The optical signal from the QCSE tuned laser was transmitted through a 2 nm bandwidth optical filter for FM slope detection. During this measurement, the phase section was kept at 0 V bias. The measured response is shown in Fig. 15. A frequency modulation 3 dB bandwidth of 10 GHz was measured, suggesting that a switching speed of 100 ps is possible with this device.

V. Conclusion

A monolithically integrated InGaAsP DBR laser using QCSE as the tuning mechanism has been demonstrated. The laser behaviour was modelled using transmission matrix equations predicting nonlinear tuning behaviour and a quasi-continuous tuning range of ~ 8 nm with the absorption peak of the tuning sections blue-shifted relatively to the lasing wavelength. Post-growth quantum well intermixing based on shallow implantation was used to blue-shift the absorption peak wavelength of the tuning sections and reduce the loss. In a non-optimised device exhibiting coupled cavity effects, non-continuous tuning across ~ 7 nm was demonstrated when the DBR voltage was varied from 0 V to -2.5 V, with ~ 20 dB SMSR and < 6 dB variation of the output power. Switching times < 3 ns were measured, limited by the switching pulse rise-time, while FM frequency response measurements suggest that 100 ps switching times would be possible with such a device.

Several improvements can be made to this device, including using implantation to isolate neighbouring sections and suppress coupled cavity effects responsible for tuning discontinuities, improving the mirror design to increase SMSR, aligning the lasing wavelength range with the wavelength range of minimum absorption change in the passive sections to reduce power fluctuations and varying separately the band-gap detuning of the passive sections to reduce tuning due to variations of the photocurrent in the phase section. Finally, considerable refractive index changes were measured across a ~ 30 nm spectral range with this device, suggesting that a design utilising multiple tuning sections could be used to offer wide tuning range.

References

[1] F.-T. An, K. S. Kim, D. Gutierrez, S. Yam, E. Hu, K. Shrikhande, and L. Kazovsky, "SUCCESS: A next-generation hybrid WDM/TDM optical access network architecture," J. Lightwave Technology, vol. 22, no. 11, pp. 2557-2569, 2004.

[2] C. Bock, J. Prat, and S. D. Walker, "Hybrid WDM/TDM PON using the AWG FSR and featuring centralised light generation and dynamic bandwidth allocation," J. Lightwave Technology, vol. 23, no. 12, pp. 3981-3988, 2005.

[3] H. Krishnamurthy, K. M. Sivalingam, and M. Mishra, "Restoration mechanisms for handling channel and link failures in optical WDM networks: tunable laser-based switch architectures and performance analysis," Computer Communications, vol. 28, pp. 987-999, 2005.

[4] Jayaraman, Z.-M. Chuang, and L. A. Coldren, "Theory, design and performance of extended tuning range semiconductor lasers with sampled

gratings," IEEE J. of Quant. Electronics, vol. 29, no. 6, pp. 1824-1834, 1993.
[5] H. Ishii, H. Tanobe, F. Kano, Y. Tohmori, Y. Kondo, and Y. Yoshikuni, "Quasicontinuous wavelength tuning in super-structure-grating (SSG) DBR lasers," IEEE J. Quant. Electronics, vol. 32, no. 3, pp. 433-441, 1996.
[6] M. Öberg, S. Nilsson, K. Streubel, J. Wallin, L. Bäckbom, and T. Klinga, "74nm wavelength tuning range of an InGaAsP/InP vertical grating assisted codirectional coupler laser with rear sampled grating reflector," IEEE Photon. Technol. Lett., vol. 15, no. 5, pp. 735-738, 1993.
[7] P.-J. Rigole, S. Nilsson, L. Bäckbom, B. Stålnacke, E. Berglind, J.-P. Weber, and B. Stoltz, "Quasi-continuous tuning range from 1560 to 1520 nm in a GCSR laser, with high power and low tuning currents," Electron. Lett., vol. 32, no. 25, pp. 2352-2354, 1996.
[8] E. Buimovich, and D. Sadot, "Physical limitation of tuning time and system considerations in implementing fast tuning of GCSR lasers," J. Lightwave Technol., vol. 22, no. 2, pp. 582-588, 2004.
[9] J. E. Simsarian, A. Bhardwaj, J. Gripp, K. Sherman, Y. Si, C. Webb, L. Zhang, and M. Zirngibl, "Fast switching characteristics of a widely tunable laser transmitter," Photon. Technol. Lett., vol. 15, no. 8, pp. 1038-1040, 2003.
[10] Y. Su, J. E. Simsarian, and L. Zhang, "Improving the switching performance of a wavelength-tunable laser transmitter using a simple and effective driver circuit," Photon. Technol. Lett., vol. 16, no. 9, pp. 2132-2134, 2004.
[11] C.-K. Chan, K. L. Sherman, and M. Zirngibl, "A fast 100-channel wavelength-tunable transmitter for optical packet switching," Photon. Technol. Lett., vol. 13, no. 7, pp. 729-731, 2001.
[12] R. O'Dowd, S. O'Duill, G. Mulvihill, N. O'Gorman, and Y. Yu, "Frequency plan and wavelength switching limits for widely tunable semiconductor transmitters," J. Selected Topics in Quant. Electron., vol. 7, no. 2, pp. 259-269, 2001.
[13] B. Puttnam, M. Dueser, and P. Bayvel, "Experimental investigation of the signal degradation in WDM transmission through coherent crosstalk caused by a fast tunable SG-DBR laser," Proc. Optical Fiber Communication Conf., Anaheim, CA, 6-11 March 2005, Paper JWA30, 2005.
[14] P. Kozodoy, T. A. Strand, Y. A. Akulova, G. Fish, C. Schow, P.-C. Koh, Z. Bian, J. Christofferson, and A. Shakouri, "Thermal effects in monolithically integrated tunable laser transmitters," IEEE Transact. On Components and Packaging Technologies, vol. 28, no 4, pp. 651-657, 2005.
[15] F. Delorme, S. Slempkes, A. Ramdane, B. Rose, and H. Nakajima, "Subnanosecond tunable Distributed Bragg Reflector lasers with an electrooptical Bragg section," IEEE J. Selected Topics in Quant. Electron., vol. 1, no. 2, pp. 396-400, 1995.
[16] G. Alibert, F. Delorme, S. Grosmaire, S. Slempkes, A. Ougazzaden, and H. Nakajima, "A new tunable laser using a single electroabsorption tuning super structure grating for subnanosecond switching applications," IEEE J. Selected Topics in Quant. Electron., vol. 3, no. 2, pp. 598-606, 1997.
[17] B. Cai, A. J. Seeds, A. Rivers, J. S. Roberts, "Multiple quantum well tuned GaAs/AlGaAs laser," Electron. Lett., vol. 25, no. 2, pp. 145-146, 1989.
[18] T. Wolf, K. Drögemüller, B. Borchert, H. Westermeier, E. Veuhoff, and H. Baumeister, "Tunable twin-guide lasers with flat frequency modulation response by quantum confined Stark effect," Appl. Phys. Lett., vol. 60, no 20, pp. 2472-2474, 1992.
[19] J. Langanay, E. Gaumont-Goarin, J. Y. Emery, C. Labourie, J. G. Provost, C. Stark, O. Le Gouézigou and D. Lesterlin, "High FM bandwidth of DBR laser including butt-koined electro-optical wavelength tuning sections," Electron. Lett., vol. 30, no 4, pp. 311-312, 1994.
[20] X. Huang, A. J. Seeds, and J. S. Roberts, "Reverse bias tuned multiple quantum well ridge guide laser with uniform frequency modulation response," Appl. Phys. Lett., vol. 71, no 6, pp. 765-766, 1997.
[21] D. A. B. Miller, D. S. Chemla, T. C. Damen, A. C. Gossard, W. Wiegmann, T. H. Wood, and C. A. Burrus, "Band-edge electroabsorption in quantum well structures: The quantum-confined Stark Effect," Phys. Rev. Lett., vol. 53, no 22, pp. 2173-2176, 1984.
[22] D. S. Chemla, D. A. B. Miller, P. W. Smith, A. C. Gossard, and W. Wiegmann, "Room temperature excitonic nonlinear absorption and refraction in GaAs/AlGaAs multiple quantum well structures," J. of Quantum Electron., vol. 20, no. 3, pp. 265-275, 1984.
[23] L. A. Coldren, and S. W. Corzine, "Diode lasers and photonics integrated circuits," Wiley Series in Microwave and Optics Engineering, 1995.
[24] S. Adachi, "Refractive indices of III-V compounds: Key properties of InGaAsP relevant to device design," J. Appl. Phys., vol. 53, no. 8, pp. 5863-5869, 1982.
[25] X. F. Liu, B. C. Qiu, M. L. Ke, A. C. Bryce, and J. H. Marsh, "Control of multiple bandgap shifts in InGaAs-AlInGaAs multiple-quantum-well material using different thicknesses of PECVD SiO_2 protection layers," IEEE Photon. Technol. Lett., vol. 12, no. 9, pp. 1141-1143, 2000.
[26] D. G. Deppe, L. J. Guido, N. Holonyak Jr, K. C. Hsieh, R. D. Burnham, R. L. Thornton, and T. L. Paoli, "Stripe-geometry quantum well heterostructure $Al_xGa_{1-x}As$-GaAs lasers defined by defect diffusion," Appl. Phys. Lett., vol. 49, no. 9, pp. 510-512, 1986.
[27] J. H. Lee, S. K. Si, Y. B. Moon, E. J. Yoon, and S. J. Kim, "Bandgap tuning of $In_{0.53}Ga_{0.47}As$/InP multiquantum well structure by impurity free vacancy diffusion using $In_{0.53}Ga_{0.47}As$ cap layer and SiO_2 dielectric capping," Electron. Lett., vol. 33, no. 13, pp.1179-1181, 1997.
[28] D. H. Yeo, K. H. Yoon, and S. J. Kim, "Characteristics of intermixed InGaAs/InGaAsP multi-quantum well structure," Jpn. J. Appl. Phys., vol. 39, pp. 1032-1034, 2000.
[29] N. Holonyak, "Impurity-induced layer disordering of quantum-well heterostructures: Discovery and Prospects," J. Select. Topics in Quantum Electronics, vol. 4, no 4, pp. 584-594, 1998.
[30] A. McKee, C. J. McLean, G. Lullo, A. C. Bryce, R. M. De La Rue, J. M. Marsh, and C. C. Button, "Monolithic integration in InGaAs-InGaAsP multiple-quantum-well structures using laser intermixing," J. of Quantum Electron., vol. 33, no. 1, pp. 45-55, 1997.
[31] B. Tell, J. Shah, P. M. Thomas, K. F. Brown-Goebeler, A. DiGiovanni, B. I. Miller, and U. Koren, "Phosphorus ion implantation induced intermixing of InGaAs-InP quantum well structures," Appl. Phys. Lett., vol. 54, no. 16, pp. 1570-1572, 1989.
[32] M. Paquette, J. Beauvais, J. Beerens, P. J. Poole, S. Charbonneau, C. J. Miner, and C. Blaauw, "Blueshifting of InGaAsP/InP laser diodes by low-energy ion implantation," Appl. Phys. Lett., vol. 71, no. 26, pp. 3749-3751, 1997.
[33] J. E. Haysom, P. G. Piva, P. J. Poole, G. C. Aers, S. Raymond, H. Chen, R. M. Feenstra, S. Charbonneau, and I. V. Mitchell, International Semiconducting and Insulating Materials Conference, pp. 197-204, 2000.
[34] E. J. Skogen, J. S. Barton, S. P. Denbaars, and L. A. Coldren, "A quantum-well-intermixing process for wavelength-agile photonics integrated circuits," J. Select. Topics in Quantum Electronics, vol. 8, no 4, pp. 863-869, 2002.
[35] J. F. Ziegler, J. P. Biersack, and U. Littmark, The Stopping and Ion Range of Ions In Matter, New York: Pergamon, 1985.
[36] M. Pantouvaki, C. P. Liu, C. C. Renaud, S. Cole, M. Robertson, R. Gwilliam, and A. J. Seeds, "Monolithically Integrated QCSE-tuned InGaAsP MQW ridge waveguide DBR laser", 18th International Conference on Indium Phosphide and Related Materials (IPRM'06), Princeton, New Jersey, USA, 7-11 May 2006, paper MA2.6.

Marianna Pantouvaki received the Degree in Physics from the University of Athens in 1998, the M.Sc. in Telecommunications in 1999 and the Ph.D. in Electronic Engineering in 2004, both from University College London.

Her Ph.D. research concerned multiple quantum well saturable absorbers with ps recovery times for high bit rate optical communications. She is currently working on semiconductor laser amplifiers integrated with saturable absorbers, Quantum Confined Stark Effect (QCSE) tunable lasers and optical comb generators, at the Ultra-Fast Photonics Group, University College London.

Cyril C. Renaud was born in Paris, France, in 1973. He received the degree of engineering from the Ecole Supérieure d'Optique, Orsay, France, and the Diplôme d'Etudes Approfondies (D.E.A.) in Optics and Photonics from the University Paris XI, Orsay, France, in 1996. He spent one year as a project engineer with Sfim-ODS, working on the development of microchips lasers. He, then, worked within Optoelectronics Research Centre, University of Southampton, Southampton UK, on diode pumped high-power ytterbium-doped fibre-lasers, with particular interest on Q-switched system and 980-nm generation. This work led to the award of a PhD in 2001.

He is currently working on optoelectronic devices and systems in the Ultra-Fast Photonics group, University College London, UK. His current research includes works on uncooled WDM sources, agile tuneable laser diode and monolithic optical frequency comb generator using Quantum Confined Stark Effect, high frequency photodetectors (UTC, travelling wave) and optical frequency generation systems in the optical and millimetre wave domains (DWDM, THZ).

Paul Cannard graduated in Metallurgy and Materials Science from University College Cardiff in 1985. He gained his PhD from Cardiff after studying Aluminium Nitride and its polytypes by atomic imaging TEM. He joined the analytical group at British Telecom Research Labs in 1988 where he used SIMS, Auger spectroscopy, TEM and SEM to study semiconductor and silica fibre based technologies. From 1996 he ran a VG80 MBE reactor growing electroabsorption modulator material and studying the potential use of antimonides as mirrors for InP based VCSELs. He transferred to Corning Research Centre in 2000 and subsequently joined CIP in 2004 as analytical scientist for epitaxial materials. He now works with an Aixtron multiwafer reactor to produce planar epitaxial material for a variety of device programmes, and with a Thomas Swan atmospheric reactor for overgrowths of buried heterostructure optoelectronic devices. He is a named inventor on one US patent (granted) and is a co-author on over 20 publications in journals and international conference proceedings.

Michael J. Robertson received the Ph.D. degree in cadmium sulphide solar cells from Durham University in 1980. After receiving the Ph.D. degree, he joined BT Labs working on GaAs laser reliability. Subsequently, he led a team that developed a high-reliability planar p–i-n photodiode and successfully transferred this to manufacturing at BT&D (now part of Agilent). During this time, he was part of the team at BT that won the Queen's Award for Technology in 1993 for its work on optoelectronic materials and devices. Since then, he has managed research on expanded mode lasers, semiconductor optical amplifiers, electroabsorption modulators, and optical switches.Within Corning Research Centre, he led the Epitaxy and Process Development teams, and is currently the III–V Technology Manager within the Centre for Integrated Photonics (CIP), Suffolk, U.K. He has published over 72 papers, filed ten patents, and written a chapter for a book on waveguide analysis.

Russel Gwilliam is the Director of Technology for the University of Surrey Ion Beam Centre. For the last 20 years he has developed advanced processes and equipment for both III-V and silicon devices and is an active consultant with several international companies. Much of his recent work has been in the area of ion beam synthesis of novel materials, including silicides in both single crystal and amorphous silicon. He is a co-inventor of the silicon light emission technology on which he founded Si-Light Technologies Ltd. He has published more than 250 papers and is a regular invited speaker at international conferences. He is a Member of both the IEE and IoP and sits on several international conference scientific committee's.

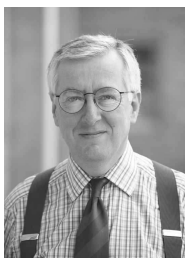

Alwyn J. Seeds received the Ph.D. and D.Sc. degrees from the University of London. From 1980 to 1983 he was a Staff Member at Lincoln Laboratory, Massachusetts Institute of Technology, where he worked on GaAs monolithic millimetre-wave integrated circuits for use in phased-array radar. He returned to England in 1983, to take up a lectureship in telecommunications at Queen Mary College, University of London, moving to University College London in 1986, where he is now Professor of Opto-electronics and Head of the Department of Electronic and Electrical Engineering. He has published over 250 papers on microwave and opto-electronic devices and their systems applications and is presenter of the video "Microwave Opto-electronics" in the IEEE Emerging Technologies series. His current research interests include microwave bandwidth tunable semiconductor lasers, semiconductor optical modulators, mode-locked lasers, optical phase-lock loops, optical frequency synthesis, broadband wireless over fiber access systems, dense WDM networks, THz photonics and non-linear optical devices.

Professor Seeds is Chairman of the Photonics Professional Network of the Institution of Engineering and Technology (UK), a Fellow of the Royal Academy of Engineering, an IEEE Fellow and a Member of the Technical Committee on Microwave Photonics of the IEEE Laser and Electro-optics Society. He has served on the programme committees for many international conferences. He is a co-founder of ZinWave Inc., a manufacturer of wireless over fibre systems.